Title
Basal resistance for three of the largest Greenland outlet glaciers

Journal
Journal of Geophysical Research Earth Surface, 121(1)

ISSN
2169-9003

Authors
Shapero, Daniel R
Joughin, Ian R
Poinar, Kristin
et al.

Publication Date
2016

DOI
10.1002/2015jf003643

Peer reviewed

AGU PUBLICATIONS

JGR

Journal of Geophysical Research: Earth Surface

RESEARCH ARTICLE
10.1002/2015JF003643

Key Points:
- The beds under three of Greenland's largest outlet glaciers provide little resistance to flow
- Changes in stress at the terminus are distributed directly to the glacier margins
- Only relatively large-scale features may be unambiguously inferred from surface observations

Correspondence to:
D. R. Shapero,
shapero@uw.edu

Citation:
Shapero, D. R., I. R. Joughin, K. Poinar, M. Morlighem, and F. Gillet-Chaulet (2016), Basal resistance for three of the largest greenland outlet glaciers, *J. Geophys. Res. Earth Surf.*, *121*, doi:10.1002/2015JF003643.

Received 15 JUN 2015
Accepted 6 JAN 2016
Accepted article online 12 JAN 2016

Basal resistance for three of the largest Greenland outlet glaciers

Daniel R. Shapero[1], Ian R. Joughin[1], Kristin Poinar[1], Mathieu Morlighem[2], and Fabien Gillet-Chaulet[3]

[1]Polar Science Center, Applied Physics Lab, University of Washington, Seattle, Washington, USA, [2]Department of Earth System Science, University of California, Irvine, California, USA, [3]Laboratoire de Glaciologie et Géophysique de l'Environnement, CNRS/Université Grenoble Alpes, Grenoble, France

Abstract Resistance at the ice-bed interface provides a strong control on the response of ice streams and outlet glaciers to external forcing, yet it is not observable by remote sensing. We used inverse methods constrained by satellite observations to infer the basal resistance to flow underneath three of the Greenland Ice Sheet's largest outlet glaciers. In regions of fast ice flow and high (>250 kPa) driving stresses, ice is often assumed to flow over a strong bed. We found, however, that the beds of these three glaciers provide almost no resistance under the fast-flowing trunk. Instead, resistance to flow is provided by the lateral margins and stronger beds underlying slower-moving ice upstream. Additionally, we found isolated patches of high basal resistivity within the predominantly weak beds. Because these small-scale (<1 ice thickness) features may be artifacts of overfitting our solution to measurement errors, we tested their robustness to different degrees of regularization.

1. Introduction

Many of Greenland's glaciers have sped up markedly over the last two decades [*Rignot and Kanagaratnam*, 2006; *Moon et al.*, 2012]. Excess ice discharge from Greenland due to accelerating glacier flow, as opposed to surface runoff, raised sea level by just over 2 mm ($739 \pm$ Gt) from 2000 to 2012 [*Enderlin et al.*, 2014]. Jakobshavn, Kangerdlugssuaq, and Helheim account for 40% of this excess discharge. In particular, Jakobshavn Isbrae has more than doubled its speed, with summertime peaks of more than 16 km/yr; it is now the fastest-flowing glacier draining the ice sheet [*Joughin et al.*, 2014].

Jakobshavn, Kangerdlugssuaq, and Helheim are marine-terminating glaciers that have either grounded termini or short (less than a few km) floating extensions. The retreat or advance of a tidewater glacier initiates both positive and negative feedback mechanisms [*Joughin et al.*, 2012]; while the glaciers studied here have increased their speed, others in Greenland have slowed down [*Moon et al.*, 2012]. Tidewater glaciers have a column-averaged pressure difference at their termini due to the density contrast at the ice-air/water interface [*Cuffey and Paterson*, 2010]. This pressure difference produces a net outward force, which is balanced at the scale of several ice thicknesses by membrane stress gradients and basal shear stress. When the glacier front retreats into deeper water, the mean pressure difference across the terminus increases, which is balanced by greater longitudinal membrane stress at the terminus [*Hughes*, 2003; *Howat et al.*, 2005]. The resulting increase in longitudinal strain rate during such a retreat stretches and thins the ice [*Thomas*, 2004; *Nick et al.*, 2009]. This thinning has several consequences. First, thinning decreases the effective pressure at the ice bed and in turn the basal resistance [*Meier and Post*, 1987]. Second, thinning near the terminus may result in a net steepening of the surface, which would increase the driving stress [*Howat et al.*, 2005]. Finally, the combination of thinning and greater extensional stresses makes the glacier more prone to iceberg calving [*Nick et al.*, 2010] and further retreat. Thus, an initial retreat can set off a feedback by producing thinning and speedup, which cause further retreat [*Thomas*, 2004]. Another basal high farther upstream may slow or stabilize this retreat but only reduces discharge to the balance flux or below.

Though the fast flow of Jakobshavn, Kangerdlugssuaq, and Helheim Glaciers is well documented, the underlying mechanisms of such flow are uncertain. Early studies of Jakobshavn Isbrae suggested that much of its motion was due to vertical shear within ice flowing over a strong bed [*Iken et al.*, 1993; *Lüthi et al.*, 2002; *Van Der Veen et al.*, 2011] which resists the horizontal sliding of ice above it. More recent results from depth-averaged ice flow models applied to Jakobshavn instead suggest that it flows over a weak bed [*Joughin et al.*, 2012;

Habermann et al., 2013]. Depth-averaged models were developed for shallow streams [*MacAyeal*, 1989; *Schoof and Hindmarsh*, 2010], which flow through deep, narrow troughs and which transition from the no-sliding to the fast-sliding regime [*Truffer and Echelmeyer*, 2003]. To rigorously address the discrepancies between the results of these studies, we used a full Stokes model to investigate the distribution of bed strength under Jakobshavn, Kangerdlugssuaq, and Helheim Glaciers.

2. Methods

The flow of ice can be modeled using the Stokes equations with a non-Newtonian constitutive law [*Cuffey and Paterson*, 2010]. The boundary condition at the ice-bedrock interface relates the shear stress τ_b along a flow line to the sliding speed u by a power law

$$\tau_b = \beta u^{\frac{1}{m}} \tag{1}$$

For many glaciers, m is found to be about 3 [*Cuffey and Paterson*, 2010], though other values are possible depending on the individual glacier and the constitution of the subglacial material, i.e., rock or till. The constant of proportionality β is the basal sliding coefficient. Our end goal is to infer the spatial distribution of τ_b. With basal shear stress parameterized as above and assuming a fixed exponent m, knowledge of both the basal sliding coefficient and the sliding velocity is sufficient to determine τ_b.

2.1. Robin Inverse Method

We use an approach outlined in *Arthern and Gudmundsson* [2010] to infer the value of β by solving a constrained optimization problem. Given an initial guess for β, two possible velocity fields can be computed which solve the Stokes equations. The first solution u^N has zero shear stress at the ice surface, i.e., it satisfies a Neumann boundary condition, but it may fail to match the observed velocities. The second solution u^D matches the observed surface velocities, i.e., it satisfies a Dirichlet boundary condition but may have unphysical surface shear stresses. The optimization problem is to minimize the functional

$$J[\beta] = \frac{1}{2}\int_\Gamma n \cdot (\sigma^N - \sigma^D) \cdot (u^N - u^D)\mathrm{d}A \tag{2}$$

where σ^N, σ^D are the full (nondeviatoric) stress tensors for the two solutions, n is the unit outward normal vector to the ice surface, and the integration is performed over the entire ice surface Γ. The minimum β of this functional produces computed velocities which best match the observed velocities and the constraint of zero surface stresses.

For our computations, we used inversion routines in the glacier modeling software Elmer/Ice [*Schäfer et al.*, 2012; *Gagliardini et al.*, 2013], which solves the full Stokes equations. Elmer/Ice has been used in a number of applications to study Greenland and marine ice sheets more generally [*Gagliardini and Zwinger*, 2008; *Pattyn et al.*, 2012; *Shannon et al.*, 2013; *Cook et al.*, 2014]. Additionally, Elmer/Ice has been compared with other similar packages through the Ice Sheet Model Intercomparison Project [*Gagliardini and Zwinger*, 2008].

The basal shear stress inferred from an inverse method will, in principle, converge to the same field regardless of the choice of sliding expontent m in equation (1) [*Joughin et al.*, 2004]. In practice, differences in the inferred basal shear stress for different values of m occur due to differing convergence rates of the resulting optimization procedure. For this study, we used $m = 1$ as this yields the most favorable convergence rate. While an inversion with a single measured velocity field cannot distinguish between linear viscous and plastic bed sliding, performing several inversions through time can; a study of Jakobshavn found that $m = 4$ provided a good fit [*Habermann et al.*, 2013].

2.2. Regularization

Although nonlinear, the transfer function for variations in basal shear stress to surface velocity and elevation is essentially a low-pass filter [*Gudmundsson*, 2003]. As in any problem of deconvolution, detailed recovery of the basal shear stress from surface observations is complicated by the fact that two basal shear stress fields with dramatically different fine-scale (<1 ice thickness) features can both give surface velocities that match observations to within the measurement error [*Habermann et al.*, 2012]. Among the large number of plausible candidate solutions for the basal shear stress, there are no criteria to determine which is the true physical field.

Instead, the best solution we can obtain is resolved only down to wavelengths which are not filtered out by the bed-to-surface transfer function. This solution can be singled out among all others using Tikhonov regularization. This method consists of adding a term proportional to the mean square gradient of β to the cost

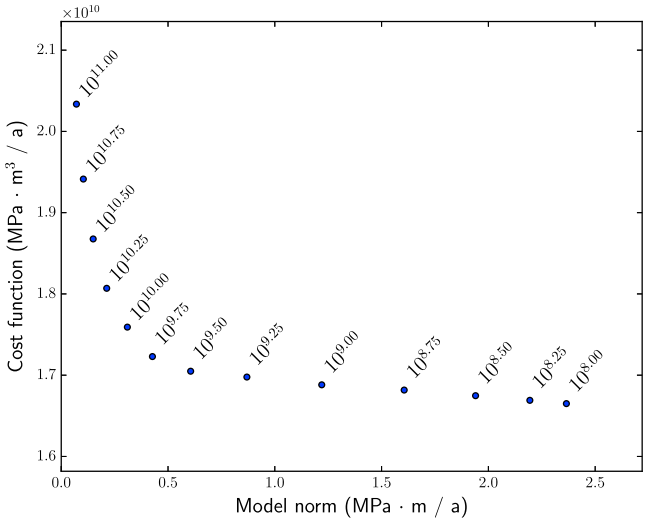

Figure 1. Cost function plotted against the mean square gradient of β for $\log_{10}\lambda = 8.0, 8.25, \ldots, 11.0$. Between $\lambda = 10^{9.75}$ and $\lambda = 10^{10}$ the cost function increases dramatically; the L-curve method would select a value in this range as the appropriate regularization parameter.

functional to penalize overly speed gradients in the basal friction coefficient. The constant of proportionality λ, which dictates the degree of smoothing used, is a free parameter that must be prescribed in some fashion. Applying too much smoothing will compromise the fit of the computed velocity to the measured velocity; applying too little smoothing will fail to eliminate potentially spurious short wavelength oscillations in the inverted basal shear stress field. Typically, as the regularization parameter λ increases, the cost function remains relatively constant up to a certain value, after which it increases sharply. This inflection point is the optimum choice for λ because it represents the maximum amount of smoothing that can be used without impairing the quality of the solution [*Hansen and O'Leary*, 1993]. To find the optimal value of the regularization parameter in accordance with this method, we performed multiple inversions for Helheim Glacier with values of λ spanning 4 orders of magnitude. These results are shown in Figure 1. The optimal value of λ depends on the signal-to-noise ratio of the measurements used to constrain the model and the number of degrees of freedom of the model, i.e., the mesh resolution [*Hansen*, 1999].

Constraining the inverted basal shear stress field to be smooth does not reflect some belief on the modeler's part that the real fields actually are smooth; indeed, basal traction may well change dramatically over short scales due to changes in water content or changes in the subglacial material. Instead, smoothing over short wavelength components of the inferred basal shear stress reflects our inability to distinguish genuine variations on this scale from spurious ones that are introduced by overfitting a solution to errors in the velocity measurements.

2.3. Observational Data

The model-data misfit is limited by errors in the velocity observations, by the errors in the surface and bed digital elevation models (DEMs) used in the model, and by the ice viscosity we prescribe.

The velocities used to constrain the inversions were computed using TerraSAR-X stripmap data. We applied a standard speckle-tracking algorithm to three image pairs for each glacier [*Joughin*, 2002]. The images were collected over periods from 16 November 2012 to 9 January 2013 (Jakobshavn), 4 December 2013 to 6 January 2014 (Kangerdlugssuaq), and 3 December 2013 to 5 January 2014 (Helheim). At each site, we averaged the multiple estimates using an error-dependent weighting [*Joughin*, 2002]. The data were posted at 100 m intervals, but the actual resolution of the smoothed offset data is only about 300 m. The absolute error in the data is about 3% and is dominated by slope-dependent errors in the surface DEM [*Joughin et al.*, 2010].

The surface elevation measurements used for Helheim and Kangerdlugssuaq were from the Greenland Ice Sheet Mapping Project (GIMP) DEM [*Howat et al.*, 2014], which has a spatial resolution of 30 m. While the GIMP DEM is nominally dated to 2007, the measurements of the ice sheet margins, where our regions of interest lie,

were collected in 2009. The surface DEM for Jakobshavn was generated from WorldView data collected in March 2013.

Several DEMs of Greenland bed topography are available, sometimes with great discrepancies among them. Resolving deep channels from sparse bedrock sounding data can be difficult due to reflections of the radar signal from the sides of the trough and from englacial water deposits. For our inversions, we used two different data sets that rely on the same source data but use different interpolation methods. The first DEM was produced by the Center for Remote Sensing of Ice Sheets (CReSIS) using standard geostatistical interpolation techniques applied to the radio echo sounding measurements [*Gogineni et al.*, 2014]. The second DEM was created using surface velocity and mass balance estimates from regional climate models to provide additional information that improves the interpolation [*Rasmussen*, 1988; *Morlighem et al.*, 2011, 2014a] rather than direct interpretation of the radio echo sounding data. In this approach, the computed bed DEM is constrained to yield an ice thickness consistent with estimates of surface elevation change and mass balance from remote sensing. Except where noted, our inversions use the Morlighem mass-conserving bed DEM.

2.4. Model for Ice Temperature and Viscosity

The viscosity of ice depends on temperature according to Arrhenius law. Throughout a glacier, the flow law parameter that determines the ice viscosity can vary by a factor as high as 12 due to thermal softening from strain heating within the ice, strain heating at the ice–bed interface, and variations in geothermal flux [*Cuffey and Paterson*, 2010]. For some glaciers, strain heating can be great enough to form a layer of ice at the pressure melting point, i.e., a temperate layer. Temperate ice often contains intragranular meltwater, which softens the ice by facilitating grain boundary sliding. Laboratory and field studies have yielded relatively diverse quantifications of the effect of meltwater on ice viscosity; we use the following parameterization from *Cuffey and Paterson* [2010]

$$E = 1 + 1.8125W \tag{3}$$

Here E is an enhancement factor and W is the perfect water content, i.e., if the volume fraction of water in an ice mass is the theoretical maximum of 1%, then the enhancement factor will be 2.8125. The presence of a temperate layer several hundred meters thick under Jakobshavn has been inferred from borehole measurements [*Iken et al.*, 1993]. The ice softness can be further enhanced by a factor of up to 2.5 in ice accumulated during the last ice age because of its high impurity content [*Paterson*, 1991].

To estimate the ice viscosity, we used a two-dimensional finite difference numerical model to calculate the thermal structure of the ice sheet, including the thickness and water content of any basal temperate ice layers [*Poinar et al.*, 2015]. The model solves the heat equation, including a source term from vertical shear heating, for temperature and water content using the approach outlined in *MacAyeal* [1997].

The model assumes the present-day geometry of the ice sheet, using basal and surface topograph from *Morlighem et al.* [2014b] and *Howat et al.* [2014], respectively. It uses regional climate model RACMO2 output for the present-day surface temperature and surface mass balance [*Ettema et al.*, 2009] and scales these values to the paleoclimate history from the Greenland Ice Sheet Project 2 (GISP2) record [*Cuffey and Clow*, 1997]. To accurately capture cold, pre-Holocene ice, the model initializes at 50 kyr before present and runs through the full deglaciation, albeit with today's ice sheet geometry. The model also uses a spatially variable geothermal flux [*Shapero and Ritzwoller*, 2004] and present-day surface velocities [*Joughin et al.*, 2010]. We use the standard rate factor for ice viscosity as a function of temperature [*Cuffey and Paterson*, 2010] and choose an enhancement factor of 3 to best approximate ice temperatures observed in the four existing Jakobshavn boreholes [*Iken et al.*, 1993; *Lüthi et al.*, 2002].

Temperatures are computed along a series of one-dimensional ice columns linked by horizontal advection from the ice divide to the glacier terminus. We run the model along tens of flow lines to obtain the temperatures in a dense set of flowbands then interpolate these to a 3-D grid. Our model considers only vertical shear heating and neglects lateral shear and longitudinal strain heating. Consequently, the model underestimates heating from flow convergence. This missing heat is concentrated in the lateral shear margins, leading to an overestimate of viscosity there. To compensate for this shortcoming, we performed an extra run with the viscosity in the shear margins enhanced by a factor of 3. Ultimately, we use the model to approximate the viscosity of the cold ice from its temperature and of the temperate ice from its liquid water content.

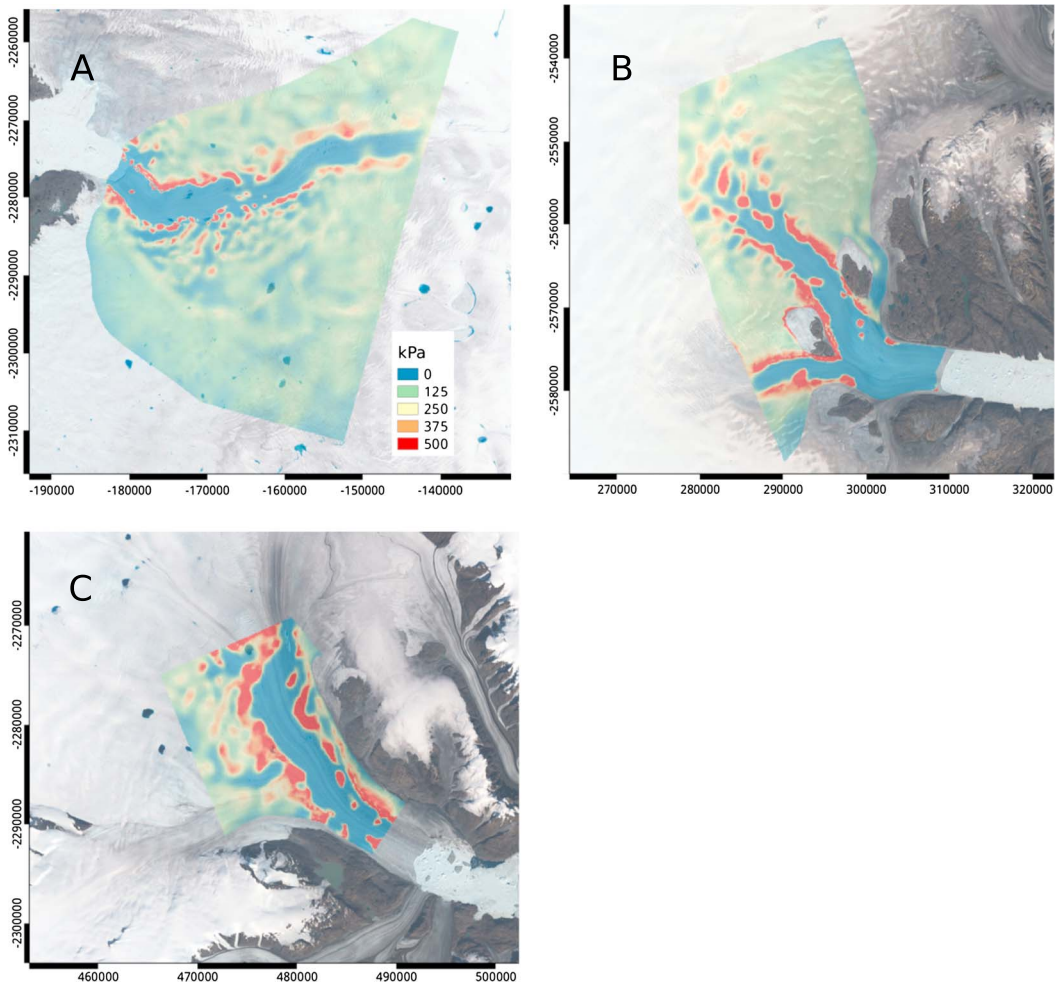

Figure 2. Basal shear stress of (a) Jakobshavn, (b) Helheim, and (c) Kangerdlugssuaq Glaciers overlain on 2014 Landsat imagery. The coordinates shown are with respect to a polar stereographic grid with a standard latitude of 70°N and longitude of 45°W.

3. Results

Using Elmer/Ice constrained by observational data, we applied the inverse method described above to approximate the bed strength under Helheim, Kangerdlugssuaq, and Jakobshavn Glaciers. These results are shown in Figure 2. For all three glaciers, our results show that in areas of fast ice flow, there is almost no frictional resistance at the bed: typical basal shear stresses are between 10 and 40 kPa, while driving stresses are on the order of several hundred kilopascals. By contrast, in regions of slower flow well away from the margins, the bed stress is comparable to the driving stress. The estimated basal shear stresses peak at ~900 kPa along the shear margins and drop precipitously under the main trunk, indicating stress transfer from the trunk of the glacier to its margins.

Over large length scales (>10 ice thicknesses), the driving stress is aligned with the flow direction. At scales on the order of an ice thickness, however, local variations in surface slope can yield driving stresses that oppose ice flow. Consequently, plotting the magnitude of the basal shear stress and comparing it with the magnitude of the driving stress without accounting for direction can obscure the true balance between these stresses. In Figure 3, we plot the component of the driving stress in the flow direction for Jakobshavn Isbrae, with positive values directed along flow. In many regions, reverse surface slopes cause the driving stress to oppose the ice flow.

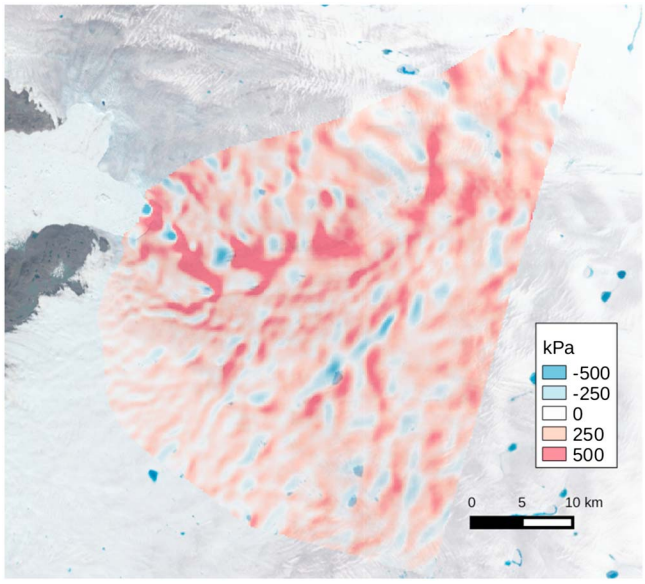

Figure 3. Component of the ice driving stress along the flow direction ($\tau_d \cdot u/\|u\|$) at Jakobshavn Isbrae. Negative values indicate driving stress opposed to flow.

3.1. Sensitivity to Surface and Basal Topography

To determine sensitivity to errors in basal topography, we inverted for basal shear stress using both the mass-conserving bed DEM [*Morlighem et al.*, 2014b] and the bed DEM produced by CReSIS [*Gogineni et al.*, 2014]. Despite significant (>100 m) discrepancies between the DEMs, we found that the bed is generally weak under the main trunk on scales greater than an ice thickness with both bed DEMs. On shorter length scales, however, the presence or absence of some features, e.g., sticky spots, depended on the specific choice of bed map. The resulting basal shear stress maps are shown in Figure 4. Similarly, using surface DEMs from GIMP and generated from WorldView imagery yielded some localized differences in basal shear stress under Jakobshavn Isbrae but did not affect our conclusion of a generally weak bed underlying the fast-flowing ice.

Despite their insensitivity to DEM choice, our results do not undermine the importance of accurate ice thickness mapping. Making predictions of future ice flow and extent requires detailed knowledge of the surface and bed topography. We are concerned only with the narrower problem of estimating subglacial bed strength

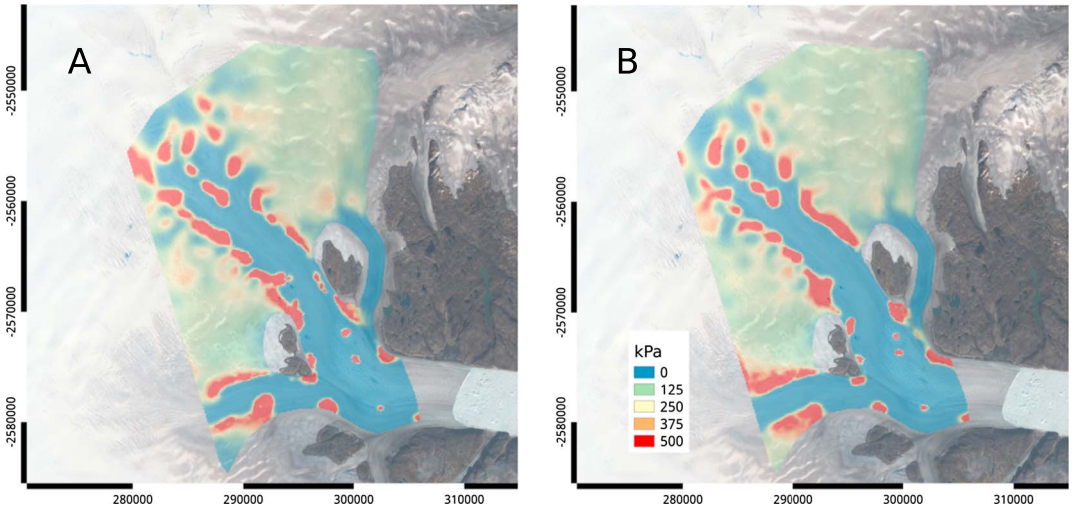

Figure 4. Inverted basal shear stress for Helheim Glacier using (a) CReSIS radar echo sounding bed DEM and (b) Morlighem mass-conserving bed DEM.

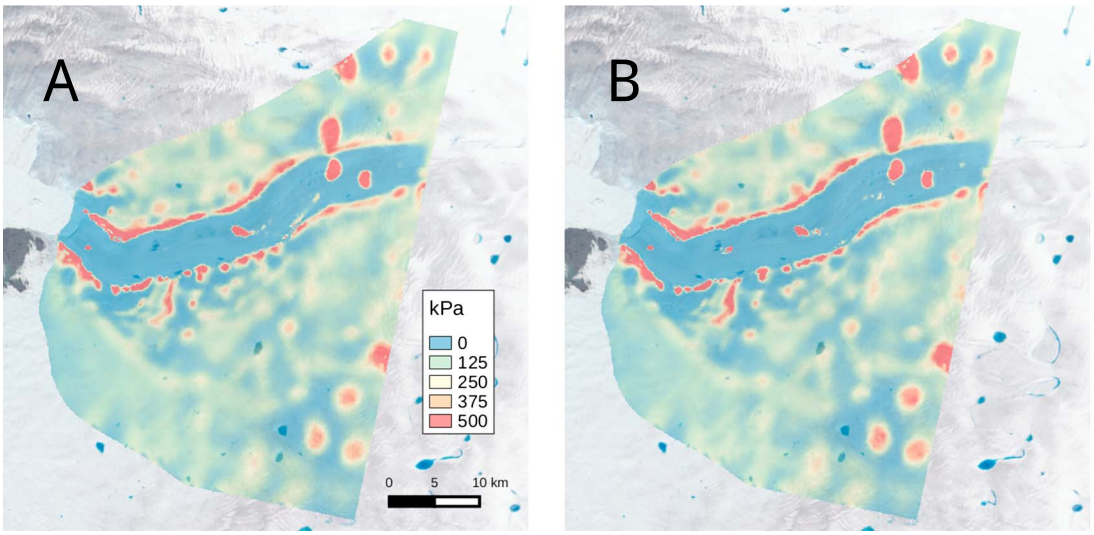

Figure 5. Inverted basal shear stress for Jakobshavn Glacier using (a) temperature model output and (b) spatially constant temperature.

at a particular time. For this problem, the response of the inferred basal shear stress at scales on the order of an ice thickness is relatively insensitive to differences in ice thickness within the range of observational errors.

3.2. Sensitivity to Ice Viscosity

We used tracers in our thermal model to identify the locations and thicknesses of ice age ice under the regions we studied then performed inversions with enhancement factors for this ice ranging from 1 to 3. The basal shear stress maps shown in Figure 2 were obtained with an enhancement factor of 3 applied to ice age ice. In the slower-flowing regions of the ice sheet surrounding the outlet glaciers, including this factor resulted in a difference of roughly 10% in the basal sliding speed but had little substantive effect on the basal shear stress. Under the main trunks of the outlet glaciers, including this factor resulted in little change in the sliding ratio, which remained high (>90%) almost everywhere. In order to examine the influence of temperature on our results, we inverted for the basal shear stress under Jakobshavn using both the temperature model output (Figure 5a) and a constant temperature of −10°C (Figure 5b), both with an enhancement factor of 3. By including the effects of temperature, the weak-bedded region is narrower but by less than half an ice thickness. In all other respects, the inverted stress fields are qualitatively similar.

3.3. Sensitivity to Model Domain

The choices of study domains were constrained by the availability of accurate velocity data in the regions of interest. While we were able to interpolate over small gaps in the velocity data at the shear margins of each glacier, gaps near the terminus of Kangerdlugssuaq Glacier could not be accurately interpolated. These missing data precluded modeling the last kilometer of Kangerdlugssuaq, which proved sensitive to details of the model initialization. For Helheim and Jakobshavn, our results were robust even when the model domain extended to the glacier termini.

Where possible, we attempted to ensure that the modeled domains are extended into slow-flowing ice outside of the main trunks of the glaciers in order to demonstrate the transfer of the driving stress to the glacier margins and to mediate any potential edge effects introduced by our choice of boundary conditions. While the available data for Jakobshavn extend far enough beyond the main trunk that this was possible, the presence of rock boundaries within the final 5–10 km of the termini of Kangerdlugssuaq and Helheim rendered this goal only partly achievable. In order to isolate genuine results from potential edge effects, we performed three additional inversions for Kangerdlugssuaq Glacier (Figure 6) with domains that cut off between 50 and 500 m from the shear margins (Figures 6b and 6d) and terminus (Figure 6c) compared to the reference domain (Figure 6a). While some small (less than an ice thickness) regions of high basal shear stress were or were not present depending on the particular model domain, overall, the results indicated that the main trunk is predominantly weak.

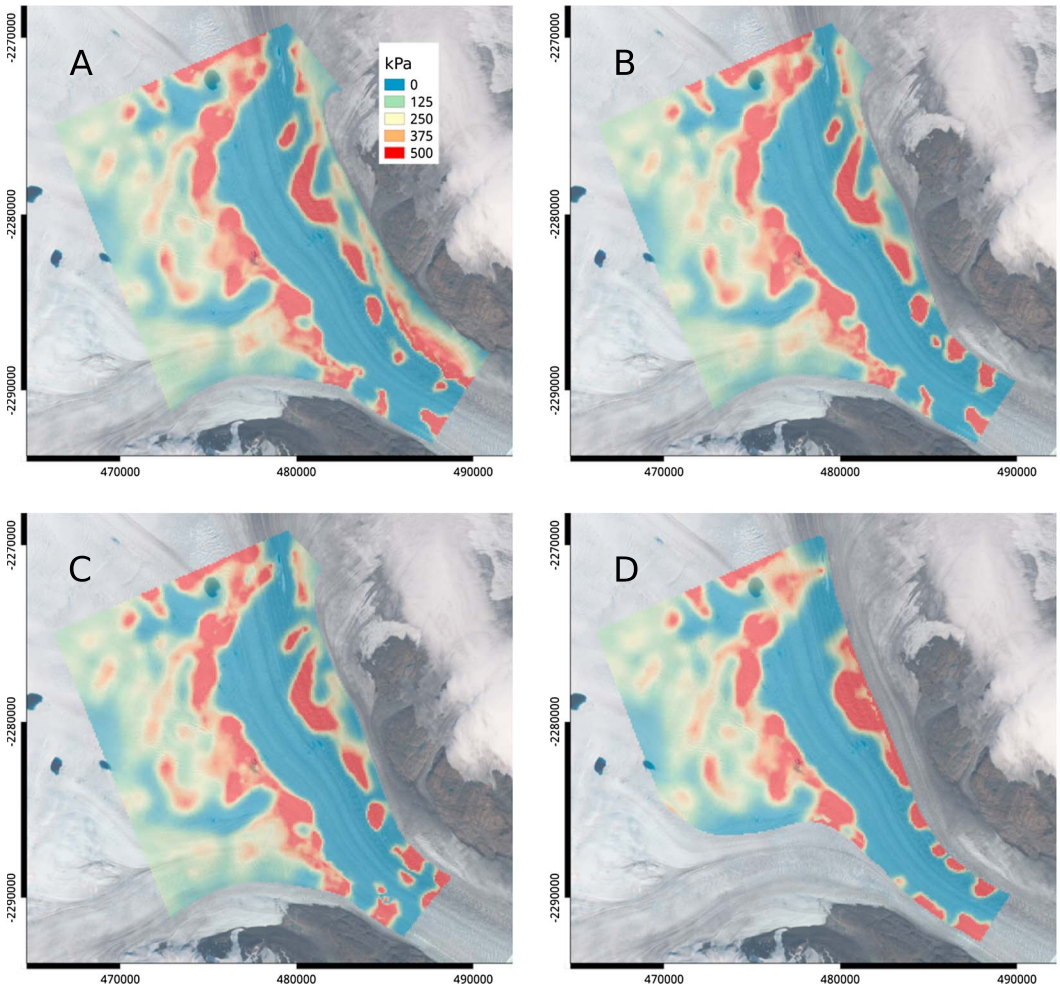

Figure 6. Basal shear stress of Kangerdlugssuaq Glacier computed on several different domains. (a) Base case domain, (b) excluding stagnant ice, (c) with less advanced frontal boundary, and (d) narrower side boundaries.

4. Discussion and Conclusions

Our results substantiate the hypothesis that the beds directly under three of Greenland's largest marine-terminating outlet glaciers support very little of the driving stress. While we have only studied three glaciers, their characteristics—flow through deeply incised bedrock troughs [*Morlighem et al.*, 2014b] and considerable velocity contrast with the surrounding ice [*Joughin et al.*, 2010; *Moon et al.*, 2012]—are common to many other glaciers in Greenland. Thus, weak beds may be a prevalent feature at the margins of the ice sheet.

The fast flow of the Siple Coast ice streams in Antarctica is attributed to slippery beds consisting of a several-meter-thick layer of weak till [*Alley et al.*, 1987]. At low effective pressures, dilatant till can behave as a Coulomb-plastic material; sliding occurs due to failure at the ice-till interface where the shear stress exceeds the till yield strength [*Tulaczyk et al.*, 2000]. Previous studies inverting for the basal shear stress of Antarctic ice streams have found that the bed supports little of the driving stress under large regions beneath Pine Island and Thwaites Glaciers [*Joughin et al.*, 2009; *Morlighem et al.*, 2010] and the ice streams feeding the Ross Ice Shelf [*Joughin et al.*, 2004]. Antarctic ice streams, however, are typically located in fairly flat regions with weak beds. The small surface slopes produce only small driving stresses, e.g., 2 kPa on Whillans Ice Stream, while the driving stresses of the major Greenland outlet glaciers can reach 250 kPa or more. Conventional wisdom has held that Greenland outlet glaciers, which typically flow through deeply incised, narrow trenches, are the opposite end member. Fast flow in Greenland has been attributed more to internal deformation, facilitated

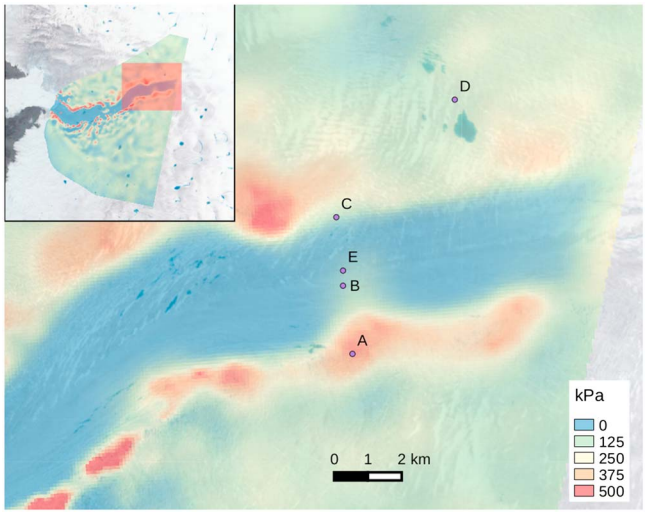

Figure 7. Basal shear stress of Jakobshavn in the vicinity of boreholes drilled by *Iken et al.* [1993] (A–C) and *Lüthi et al.* [2002] (D and E).

by high strain heating that softens the ice, with the beds supporting a large proportion of the driving stress [*Truffer and Echelmeyer*, 2003].

Our results instead suggest that weak beds are common to both Greenland and Antarctica and that the outlet glaciers of both ice sheets flow largely via sliding of the fast-flowing glacier trunks. This is possible despite the large driving stresses of Greenland Glaciers because the narrow troughs (~2 ice thicknesses) where these stresses are concentrated allow the lateral margins to balance the driving stress.

Earlier studies [*Iken et al.*, 1993; *Lüthi et al.*, 2002] asserted that the fast flow of Jakobshavn is primarily due to vertical deformation. This conclusion was based on measurements from boreholes (A–E in Figure 7) drilled 50 km upstream of the Jakobshavn terminus. In Figure 7, we plot the inferred basal shear stress in the vicinity of these boreholes. In agreement with these measurements, we find high vertical deformation rates near boreholes A and C, likely because these points occur where the margins begin to support the driving stress. At sites B and E, our inversions find a local basal shear stress maximum of roughly 65 kPa within a surrounding field of ~10 kPa. This basal shear stress is still appreciably smaller than the driving stress of ~300 kPa. At site D, *Lüthi et al.* [2002] measured a basal sliding speed to surface speed ratio of 60%; we found a sliding ratio of 70%. Given that this is within the uncertainty in the sliding ratio due to parameterizations for the softness of ice age ice, which ultimately had little effect on our findings of low basal shear stress, our estimates appear to be in rough agreement with their observations.

Previous studies using flowband models for ice flow have also suggested high vertical deformation rates within the main trunk of Jakobshavn [*Funk et al.*, 1994; *Lüthi et al.*, 2002]. These models, however, parameterize lateral stresses; our results suggest that since the glacier shear margins support so much of the driving stress, this component of the stress field is important to model explicitly.

New evidence has found that several of Greenland's outlet glaciers are underlain by deformable till [*Dow et al.*, 2013; *Walter et al.*, 2014]. Gravity surveys also suggest the presence of a deep layer of soft till in much of the Jakobshavn trough [*Block and Bell*, 2011]. Additionally, time-dependent inversions for Jakobshavn from 1995 to 2006 have shown that the yield strength of its bed may have decreased since its speedup began in 2003 [*Habermann et al.*, 2013], possibly due to thinning that brought the glacier closer to flotation. Thus, we hypothesize that the weak beds indicated by the inversions may be due to a weak dilatant till at low effective pressure. Alternatively, the subglacial hydrological system may provide sufficient lubrication for the ice to slide rapidly regardless of the underlying material. If this is the case, the subglacial hydrological system would be at low effective pressure with an inefficient drainage network [*Cuffey and Paterson*, 2010]. Strong seasonal input of meltwater to the bed might then cause a late-summer transition to an efficient drainage network, producing an abrupt late-summer ice slowdown [*Howat et al.*, 2010]. Since no such slowdown is observed [*Echelmeyer and Harrison*, 1990; *Joughin et al.*, 2008], our preferred hypothesis is that Jakobshavn, Kangerdlugssuaq, and Helheim Glaciers are underlain by weak dilatant till at low effective pressure year round.

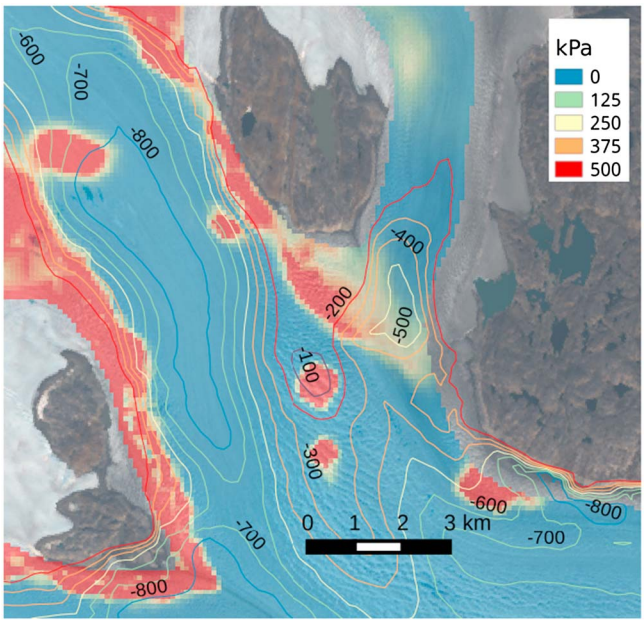

Figure 8. Bed elevation contours and stress of Helheim Glacier. The −100 m elevation contour coincides with a sticky spot.

Weakening of the shear margins of Jakobshavn Isbrae through crevassing and meltwater penetration has been proposed as an important control on its speed [*Van Der Veen et al.*, 2011]. Incorporating the effects of crevasse formation and meltwater percolation into a glacier model would, however, entail the inclusion of even more underconstrained quantities, such as strain history, into the ice physics. While ice weakening in the shear margins would reduce stresses transverse to the flow direction, this would require higher longitudinal stresses in the main trunk for the glacier to remain in balance. To approximate the effect of large-scale damage and crevassing within the ice shear margins, *Joughin et al.* [2012] used both a reference rheology and weaker shear margins with an enhancement factor of 8 in inversions for Jakobshavn Isbrae. Although the area of the weak-bedded region was slightly different when the shear margins were softened, the basal shear stress field was not substantially different from the stronger case [*Joughin et al.*, 2012]. A weak bed under large areas of the main glacier trunks thus remains a robust explanation for observed ice flow in Greenland.

Each of our inversions features small sliding-resistant regions within the otherwise fast-sliding trunk. Some of these areas of high basal resistance correspond to bedrock highs extending over regions ~1 km wide [*Alley*, 1993], as shown in Figure 8. The local sensitivity of the inverted stress field to relatively small-scale features of the bed topography underscores the need for accurate mapping of Greenland's bed elevation at a resolution equal to or higher than the desired resolution of glacier bed stress maps. For the purposes of this study, however, we are primarily concerned with spatial scales larger than that of an individual sticky spot.

There are other areas of sharp velocity gradients in the main trunks of both Helheim and Kangerdlugssuaq that lack concomitant features in either the surface or bed elevation and which, according to our inversions, are underlain by sticky spots. A different mechanism, such as till discontinuity [*Alley*, 1993], may be responsible for these features.

While some of the sticky spots we found persisted in every inversion, others varied in location and size depending on the initial guess for the basal sliding coefficient, the particular choice of bed DEM, and other model parameters. These features, even when robust to changes in the model parameters, may be more localized than our inversions suggest; i.e., a delta function-like disturbance in the true basal shear stress would appear as a Gaussian with some finite width in the inferred basal shear stress.

The bed stress field we computed for Jakobshavn is in broad agreement with previous studies [*Joughin et al.*, 2012; *Habermann et al.*, 2013] but differs from that of *Sergienko et al.* [2014]. Where we have relatively smooth areas of high or low bed stress interspersed with sparse sticky spots, they find 5–20 km long, banded structures in the stress field spaced at ~2–3 km intervals. However, *Sergienko et al.* [2014] found that the periodicity

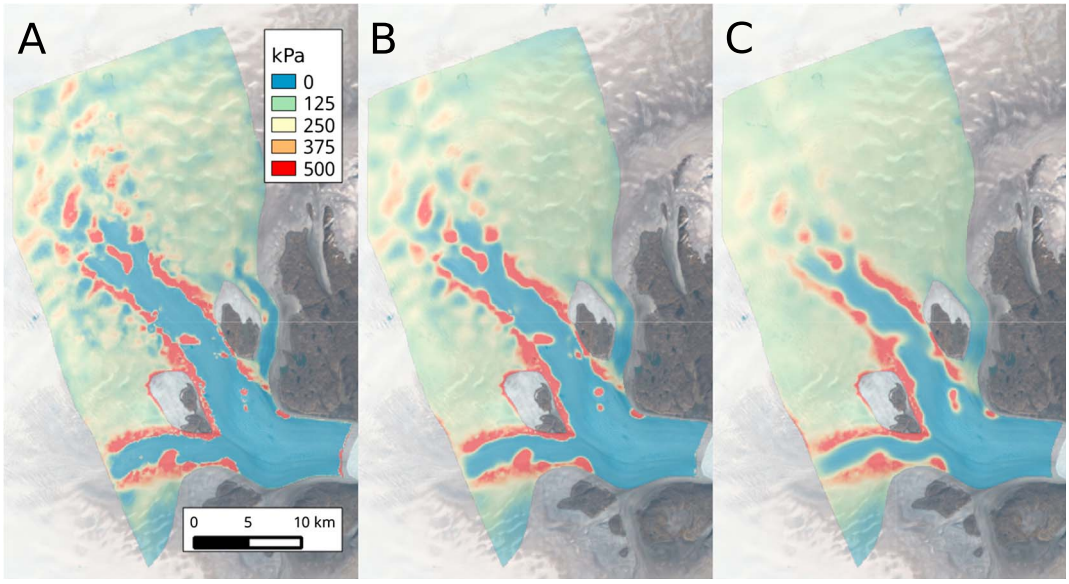

Figure 9. Basal shear stress of Helheim Glacier with different values of the regularization parameter: (a) $\lambda = 10^9$, (b) $\lambda = 10^{10}$, and (c) $\lambda = 10^{11}$. With $\lambda = 10^9$, the inferred basal shear stress exhibits short wavelength features that may indistinguishable from fitting to measurement errors. Using $\lambda = 10^{11}$, the computed solution no longer provides an adequate fit to the data.

and scale of these banded structures vary depending on the choice of the regularization parameter used in the inversion. Our computed basal shear stress field also exhibits fine-scale features at low values of the regularization parameter (Figure 9). While the fine-scale features that *Sergienko et al.* [2014] find may well be present under real glaciers, we assert that the computed basal response to imperfect surface observations limits the extent to which these features can be inferred with certainty; there are other solutions without such features that produce equally plausible matches to the data, as in Figures 9a and 9b.

Our results show that the beds under three of Greenland's most prominent outlet glaciers provide little resistance to the driving stress. The regions where we find weak beds coincide with the areas of fast flow and rapid thinning [*Howat et al.*, 2007; *Pritchard et al.*, 2009]. Thus, it is likely that that bed strength has a substantial effect on the overall ice dynamics and is important to accurately represent in models used to project sea level contributions from the Greenland Ice Sheet. The glaciers we have considered may be more broadly representative of the ~200 others that drain the ice sheet, many of which flow rapidly through deep troughs and have exhibited similar patterns of retreat and thinning [*Moon et al.*, 2012]. If this is indeed the case, much of the Greenland Ice Sheet could be vulnerable to the climate-induced mass loss that has been observed on Jakobshavn, Helheim, and Kangerdlugssuaq.

Acknowledgments
The authors wish to thank Rupert Gladstone, two anonymous reviewers and the Associate Editor for their helpful contributions in improving the manuscript. NSF supported the contributions of D.S., I.J., and K.P. through the Center for Remote Sensing of Ice Sheets (CReSIS) (NSF ANT-0424589). We acknowledge NASA's Operation IceBridge (bed elevation), the German Space Agency (TerraSAR-X data), and I. Howat (email: howat.4@osu.edu) who provided much of the data used to constrain the model (GIMP DEM funded by NASA MEaSUReSNNX08AL98A). Ice sheet velocity products were processed under NASA MEaSUREs (NNX08AL98A). The velocity and bed elevation data for this paper are available from the National Snow and Ice Data Center (http://www.nsidc.org), and the surface elevation data are available from the Byrd Polar Research Center (http://bpcrc.osu.edu/gdg/data/gimpdem). All codes used in the preparation of this manuscript are publicly available at http://github.com/danshapero/greenland_inversions.git.

References

Alley, R. B. (1993), In search of ice-stream sticky spots, *J. Glaciol.*, *39*, 447–454.
Alley, R. B., D. D. Blankenship, C. R. Bentley, and S. T. Rooney (1987), Till beneath ice stream B: 3. Till deformation—Evidence and implications, *J. Geophys. Res.*, *92*(B9), 8921–8929.
Arthern, R. J., and G. H. Gudmundsson (2010), Initialization of ice-sheet forecasts viewed as an inverse Robin problem, *J. Glaciol.*, *56*(197), 527–533.
Block, A. E., and R. E. Bell (2011), Geophysical evidence for soft bed sliding at Jakobshavn Isbrae, West Greenland, *Cryosphere Discuss.*, *5*(1), 339–366.
Cook, S., I. C. Rutt, T. Murray, A. Luckman, T. Zwinger, N. Selmes, A. Goldsack, and T. D. James (2014), Modelling environmental influences on calving at Helheim Glacier in eastern Greenland, *Cryosphere*, *8*(3), 827–841.
Cuffey, K. M., and G. D. Clow (1997), Temperature, accumulation and ice sheet elevation in central Greenland through the last deglacial transition, *J. Geophys. Res.*, *102*, 26,383–26,396.
Cuffey, K. M., and W. S. B. Paterson (2010), *The Physics of Glaciers*, Acad. Press, Cambridge, Mass..
Dow, C. F., A. Hubbard, A. D. Booth, S. H. Doyle, A. Gusmeroli, and Y. B. Kulessa (2013), Seismic evidence of mechanically weak sediments underlying Russell Glacier, West Greenland, *Ann. Glaciol.*, *54*(64), 135–141.
Echelmeyer, K., and W. Harrison (1990), Jakobshavns Isbrae, West Greenland: Seasonal variations in velocity - or lack thereof, *Ann. Glaciol.*, *36*(122), 82–88.
Enderlin, E. M., I. M. Howat, S. Jeong, M.-J. Noh, J. H. van Angelen, and M. R. van den Broeke (2014), An improved mass budget for the Greenland ice sheet, *Geophys. Res. Lett.*, *41*, 866–872, doi:10.1002/2013GL059010.

Ettema, J., M. R. van den Broeke, E. van Meijgaard, W. J. van de Berg, J. L. Bamber, J. E. Box, and R. C. Bales (2009), Higher surface mass balance of the Greenland ice sheet revealed by high-resolution climate modeling, *Geophys. Res. Lett.*, *36*, L12501, doi:10.1029/2009GL038110.
Funk, M., K. Echelmeyer, and A. Iken (1994), Mechanisms of fast flow in Jakobshavns Isbrae, West Greenland: Part II. Modeling of englacial temperatures, *J. Glaciol.*, *40*(136), 569–585.
Gagliardini, O., and T. Zwinger (2008), The ISMIP-HOM benchmark experiments performed using the finite-element code Elmer, *Cryosphere Discuss.*, *2*(1), 75–109.
Gagliardini, O., et al. (2013), Capabilities and performance of Elmer/Ice, a new generation ice-sheet model, *Geosci. Model Dev.*, *6*, 1299–1318.
Gogineni, S., et al. (2014), Bed topography of Jakobshavn Isbræ, Greenland, and Byrd Glacier, Antarctica, *J. Glaciol.*, *60*, 813–833.
Gudmundsson, G. H. (2003), Transmission of basal variability to a glacier surface, *J. Geophys. Res.*, *108*(B5), 2253, doi:10.1029/2002JB002107.
Habermann, M., D. Maxwell, and M. Truffer (2012), Reconstruction of basal properties in ice sheets using iterative inverse methods, *J. Glaciol.*, *58*(210), 795–807.
Habermann, M., M. Truffer, and D. Maxwell (2013), Changing basal conditions during the speed-up of Jakobshavn Isbræ, Greenland, *Cryosphere Discuss.*, *7*(3), 2153–2190.
Hansen, P., and D. O'Leary (1993), The use of the L-curve in the regularization of discrete ill-posed problems, *SIAM J. Sci. Comput.*, *14*(6), 1487–1503.
Hansen, P. (1999), *The L-Curve and Its Use in the Numerical Treatment of Inverse Problems*, IMM, Dep. of Math. Modell., Tech. Univ. of Denmark, Denmark.
Howat, I. M., I. Joughin, S. Tulaczyk, and S. Gogineni (2005), Rapid retreat and acceleration of Helheim Glacier, east Greenland, *Geophys. Res. Lett.*, *32*, L22502, doi:10.1029/2005GL024737.
Howat, I. M., I. Joughin, and T. Scambos (2007), Rapid changes in ice discharge from Greenland outlet glaciers, *Science*, *315*(5818), 1559–1561.
Howat, I. M., J. E. Box, Y. Ahn, A. Herrington, and E. M. McFadden (2010), Seasonal variability in the dynamics of marine-terminating outlet glaciers in Greenland, *J. Glaciol.*, *56*(198), 601–613.
Howat, I. M., A. Negrete, and B. E. Smith (2014), The Greenland Ice Mapping Project (GIMP) land classification and surface elevation datasets, *Cryosphere Discuss.*, *8*(1), 453–478.
Hughes, T. (2003), Geometrical force balance in glaciology, *J. Geophys. Res.*, *108*(B11), 2526, doi:10.1029/2003JB002557.
Iken, A., K. Echelmeyer, W. Harrison, and M. Funk (1993), Mechanisms of fast flow in Jakobshavns Isbræ, West Greenland. I: Measurements of temperature and water level in deep boreholes, *J. Glaciol.*, *39*(131), 15–25.
Joughin, I. (2002), Ice-sheet velocity mapping: A combined interferometric and speckle-tracking approach, *Ann. Glaciol.*, *34*(1), 195–201.
Joughin, I., D. R. MacAyeal, and S. Tulaczyk (2004), Basal shear stress of the Ross ice streams from control method inversions, *J. Geophys. Res.*, *109*, B09405, doi:10.1029/2003JB002960.
Joughin, I., S. B. Das, M. A. King, B. E. Smith, I. M. Howat, and T. Moon (2008), Seasonal speedup along the western flank of the Greenland ice sheet, *Science*, *320*(5877), 781–783.
Joughin, I., S. Tulaczyk, J. L. Bamber, D. Blankenship, J. W. Holt, T. Scambos, and D. G. Vaughan (2009), Basal conditions for Pine Island and Thwaites Glaciers, West Antarctica, determined using satellite and airborne data, *J. Glaciol.*, *55*(190), 245–257.
Joughin, I., B. E. Smith, I. M. Howat, T. Scambos, and T. Moon (2010), Greenland flow variability from ice-sheet-wide velocity mapping, *J. Glaciol.*, *56*(197), 415–430.
Joughin, I., B. E. Smith, I. M. Howat, D. Floricioiu, R. B. Alley, M. Truffer, and M. Fahnestock (2012), Seasonal to decadal scale variations in the surface velocity of Jakobshavn Isbrae, Greenland: Observation and model-based analysis, *J. Geophys. Res.*, *117*, F02030, doi:10.1029/2011JF002110.
Joughin, I., B. E. Smith, D. E. Shean, and D. Floricioiu (2014), Brief communication: Further summer speedup of Jakobshavn Isbræ, *Cryosphere*, *8*(1), 209–214.
Lüthi, M., M. Funk, A. Iken, S. Gogineni, and M. Truffer (2002), Mechanisms of fast flow in Jakobshavn Isbrae, West Greenland: Part III. Measurements of ice deformation, temperature and cross-borehole conductivity in boreholes to the bedrock, *J. Glaciol.*, *48*(162), 369–385.
MacAyeal, D. R. (1989), Large-scale ice flow over a viscous basal sediment: Theory and application to Ice Stream B, Antarctica, *J. Geophys. Res.*, *94*(B4), 4071–4087.
MacAyeal, D. R. (1997), EISMINT: Lessons in ice-sheet modeling, *Tech. Rep.*, Univ. of Chicago, Dep. of Geophys. Sci., Chicago, IL.
Meier, M. F., and A. Post (1987), Fast tidewater glaciers, *J. Geophys. Res.*, *92*(B9), 9051–9058.
Moon, T., I. Joughin, B. Smith, and I. Howat (2012), 21st-century evolution of Greenland outlet glacier velocities, *Science*, *336*(6081), 576–578.
Morlighem, M., E. Rignot, H. Seroussi, E. Larour, H. Ben Dhia, and D. Aubry (2010), Spatial patterns of basal drag inferred using control methods from a full-Stokes and simpler models for Pine Island Glacier, West Antarctica, *Geophys. Res. Lett.*, *37*, L14502, doi:10.1029/2010GL043853.
Morlighem, M., E. Rignot, H. Seroussi, E. Larour, H. Ben Dhia, and D. Aubry (2011), A mass conservation approach for mapping glacier ice thickness, *Geophys. Res. Lett.*, *38*, L19503, doi:10.1029/2011GL048659.
Morlighem, M., E. Rignot, J. Mouginot, H. Seroussi, and E. Larour (2014a), High-resolution ice-thickness mapping in South Greenland, *Ann. Glaciol.*, *55*(67), 64–70.
Morlighem, M., E. Rignot, J. Mouginot, H. Seroussi, and E. Larour (2014b), Deeply incised submarine glacial valleys beneath the Greenland ice sheet, *Nat. Geosci.*, *7*, 418–422.
Nick, F. M., A. Vieli, I. M. Howat, and I. Joughin (2009), Large-scale changes in Greenland outlet glacier dynamics triggered at the terminus, *Nat. Geosci.*, *2*(2), 110–114.
Nick, F. M., C. J. van der Veen, A. Vieli, and D. I. Benn (2010), A physically based calving model applied to marine outlet glaciers and implications for the glacier dynamics, *J. Glaciol.*, *56*(199), 781–794.
Paterson, W. S. B. (1991), Why ice-age ice is sometimes "soft", *Cold Reg. Sci. Technol.*, *20*, 75–98.
Pattyn, F., et al. (2012), Results of the marine ice sheet model intercomparison project, MISMIP, *Cryosphere*, *6*(3), 573–588.
Poinar, K., I. Joughin, S. B. Das, M. D. Behn, J. Lenaerts, and M. R. Broeke (2015), Limits to future expansion of surface-melt-enhanced ice flow into the interior of western Greenland, *Geophys. Res. Lett.*, *42*, 1800–1807, doi:10.1002/2015GL063192.
Pritchard, H. D., R. J. Arther, D. G. Vaughin, and L. A. Edwards (2009), Extensive dynamic thinning on the margins of the Greenland and Antarctic ice sheets, *Nature*, *461*(7266), 971–975.
Rasmussen, L. A. (1988), Bed topography and mass-balance distribution of Columbia Glacier, Alaska, USA, determined from sequential aerial photography, *J. Glaciol.*, *34*, 208–216.
Rignot, E., and P. Kanagaratnam (2006), Changes in the velocity structure of the Greenland Ice Sheet, *Science*, *311*(5763), 986–990.

Schäfer, M., T. Zwinger, P. Christoffersen, F. Gillet-Chaulet, K. Laakso, R. Pettersson, V. A. Pohjola, T. Strozzi, and J. C. Moore (2012), Sensitivity of basal conditions in an inverse model: Vestfonna ice-cap, Nordaustlandet/Svalbard, *Cryosphere*, *6*, 771–783.

Schoof, C., and R. C. A. Hindmarsh (2010), Thin-film flows with wall slip: An asymptotic analysis of higher order glacier flow models, *Q. J. Mech. Appl. Math.*, *63*, 73–114.

Sergienko, O. V., T. T. Creyts, and R. C. A. Hindmarsh (2014), Similarity of organized patterns in driving and basal stresses of Antarctic and Greenland ice sheets beneath extensive areas of basal sliding, *Geophys. Res. Lett.*, *41*, 3925–3932, doi:10.1002/2014GL059976.

Shannon, S. R., et al. (2013), Enhanced basal lubrication and the contribution of the Greenland ice sheet to future sea-level rise, *Proc. Natl. Acad. Sci. USA*, *110*(35), 14,156–14,161.

Shapero, N. M., and M. H. Ritzwoller (2004), Inferring surface heat flux distributions guided by a global seismic model: Particular application to Antarctica, *Earth Planet. Sci. Lett.*, *223*(1–2), 213–224.

Thomas, R. H. (2004), Force-perturbation analysis of recent thinning and acceleration of Jakobshavn Isbrae, Greenland, *J. Glaciol.*, *50*(168), 57–66.

Truffer, M., and K. A. Echelmeyer (2003), Of Isbrae and ice streams, *Ann. Glaciol.*, *36*(1), 66–72.

Tulaczyk, S., W. B. Kamb, and H. F. Engelhardt (2000), Basal mechanics of ice stream B, West Antarctica: 1. Till mechanics, *J. Geophys. Res.*, *105*(B1), 463–481.

Van Der Veen, C. J., J. C. Plummer, and L. A. Stearns (2011), Controls on the recent speed-up of Jakobshavn Isbrae, West Greenland, *J. Glaciol.*, *57*(204), 770–782.

Walter, F., J. Chaput, and M. P. Lüthi (2014), Thick sediments beneath Greenland's ablation zone and their potential role in future ice sheet dynamics, *Geology*, *42*(6), 487–490.